An Iron Reservoir Model Based on Ferrichrome: Iron(III)-Binding and Metal(III)-Exchange Properties of Tripodal Monotopic and Ditopic Hydroxamate Ligands with an L-Alanyl-L-alanyl-*N*-hydroxy-β-alanyl Sequence

Yukihiro Hara and Masayasu Akiyama*

Contribution from the Department of Applied Chemistry, Tokyo University of Agriculture and Technology, Koganei, Tokyo 184-8588, Japan

Received September 1, 2000

Abstract: To gain knowledge about biological iron mobilization, tripodal monotopic and ditopic hydroxamate ligands (**1** and **2**) are prepared, and their iron-chelating properties are investigated. Ligands **1** and **2** contain three Ala-Ala-β-(HO)Ala units and three [Ala-Ala-β-(HO)Ala]$_2$ units connected with tris(alanylaminoethyl)-amine, respectively, and form six-coordinate octahedral complexes with iron(III) in aqueous solution. Ligand **1** and 1 equiv of iron give Fe-**1**, and ligand **2** and 1 or 2 equiv of iron produce Fe_1-**2**, or Fe_2-**2**. These complexes exhibit absorptions at λ_{max} 425 nm of ϵ 2800−3000/Fe, characteristic of tris(hydroxamato)iron(III) complexes, and preferentially assume the Δ-*cis* configuration. Loading of Fe(III) on **1**, **2**, and M(III)-loaded ligands (M-**1** and M_1-**2**, M = Al, Ga, In) with ammonium ferric oxalate at pH 5.4 is performed, and the second-order rate constants of loading with respect to Fe(III) and the ligand or M(III)-loaded ligands are determined. The rates of loading of Fe(III) on M-**1** increase in the order Al-**1** < Ga-**1** < In-**1**, and those on M_1-**2** in the order Al_1-**2** < Ga_1-**2** < Fe_1-**2** < In_1-**2**, indicating that the dissociation tendency of M(III) ions from the hydroxamate ligand is an important factor. The iron complexes formed with **2** are subjected to an iron removal reaction with excess EDTA in aqueous pH 5.4 solution at 25.0 °C, and the collected data are analyzed by curve-fitting using appropriate first-order kinetic equations, providing the rate constants for the upper site and the lower site of **2**. Similar analysis for FeM-**2** affords removal rate constants for Fe^{up}-**2**, M^{up}-**2**, and Fe^{low}-**2**, and the iron residence probability at each site. The protonation constants of the hydroxamate groups for **1** and **2** (pK_1, pK_2, pK_3, and pK_1, pK_2 ..., pK_6) are determined, and the proton-independent stability constants for Fe-**1**, the upper site of Fe_2-**2**, and the lower site of Fe_1-**2** are 10^{28}, 10^{29}, and $10^{28.5}$, respectively.

Introduction

Iron is an essential element for almost all living organisms, but its availability is limited due to the formation of insoluble ferric oxide polymers.[1] In response, organisms have developed efficient systems for iron capture, storage, and release.[1−3] In mammals, iron is absorbed from digested food and carried by transferrin to various locations for utilization[4,5] or to ferritin for storage.[6−8] Microorganisms use siderophores (low-molecular weight, chelating compounds) to sequester iron from the environment, and siderophore−iron complexes are transported into cells, where the iron is released.[9−12] Description of biological iron transport and storage processes requires a profound knowledge of iron mobilization by ligand−metal exchange. In this respect, the design and synthesis of artificial iron(III)-storing compounds, in particular, multitopic iron-binding compounds, and evaluation of their iron-binding properties would help us to better understand the intricate processes of biological iron mobilization.[1]

We chose ferrichrome as a prototype for designing iron-storing compounds. Ferrichrome is the iron(III) complex of a representative exocyclic tripodal hydroxamate siderophore,[9,10] and its characteristic properties have been elucidated through studies of microbial iron transport,[9,10] X-ray analysis,[13,14] NMR

(1) (a) Crichton, R. R. *Inorganic Biochemistry of Iron Metabolism*; Ellis Horwood: Chichester, 1991. (b) Crichton, R. R.; Ward, R. J. *Analyst* **1995**, *120*, 693−697.

(2) Fatemi, S. J. A.; Kadir, F. H. A.; Williamson, D. J.; Moore, G. R. *Adv. Inorg. Chem.* **1991**, *36*, pp 409−448.

(3) Kaim, W.; Schwederski, B. *Bioinorganic Chemistry: Inorganic Elements in the Chemistry of Life*; John Wiley & Sons: Chichester, 1994.

(4) Baker, E. N.; Lindley, P. F. *J. Inorg. Biochem.* **1992**, *47*, 147−160.

(5) Aisen, P. In *Metal Ions in Biological Systems*; Sigel, A., Sigel, H., Eds.; Marcel Dekker: New York, 1998; Vol. 35, pp 585−632.

(6) Theil, E. C.; Aisen, P. In *Iron Transport in Microbes, Plants and Animals;* Winkelmann, G., van der Helm, D., Neilands, J. B., Eds.; VCH Publishers: Weinheim, 1987; pp 491−520.

(7) Harrison, P. M.; Andrews, S. C.; Artymiuk, P. J.; Ford, G. C.; Guest, J. R.; Hirzmann, J.; Lowson, D. M.; Livingstone, J. C.; Smith, J. M. A.; Treffry, A.; Yewdall, S. J. *Adv. Inorg. Chem.* **1991**, *36*, 449−486.

(8) Chasteen, N. D. In *Metal Ions in Biological Systems*; Sigel, A., Sigel, H., Eds.; Marcel Dekker: New York, 1998; Vol. 35, pp 479−514.

(9) (a) Neilands, J. B. In *Microbial Iron Metabolism*; Neilands, J. B., Ed.; Academic Press: New York, 1974; pp 3−34. (b) Bagg, A.; Neilands, J. B. *Microbiol. Rev.* **1987**, *51*, 509−518.

(10) (a) Emery, T. In *Metal Ions in Biological Systems*; Sigel, H., Ed; Marcel Dekker: New York, 1978; Vol. 7, pp 77−126. (b) Emery, T. In *Iron Transport in Microbes, Plants and Animals*; Winkelmann, G., van der Helm, D., Neilands, J. B., Eds.; VCH Publishers: Weinheim, 1987; pp 235−250.

(11) (a) Raymond, K. N.; Müller, G.; Matzanke, B. F. *Top. Curr. Chem.* **1984**, *123*, 49−102. (b) Matzanke, B. F.; Müller-Matzanke, G.; Raymond, K. N. In *Iron Carriers and Iron Proteins*; Loehr, T. M., Ed.; Physical Bioinorganic Chemistry Series, Vol. 5; VCH Publishers: New York, 1989; pp 3−121.

(12) Matzanke, B. F. In *Encyclopedia of Inorganic Chemistry*; King, R. B., Ed.; John Wiley & Sons: Chichester, 1994; Vol. 4, pp 1915−1932.

(13) Zalkin, A.; Forrester, J. D.; Templeton, D. H. *J. Am. Chem. Soc.* **1966**, *88*, 1810−1814.

10.1021/ja003251g CCC: $20.00
Published on Web 07/10/2001

spectroscopy,[15] iron-transport experiments,[9a] and iron-exchange kinetics.[16] Recently, a ferrichrome family has even been suggested as an iron-storing vehicle for a microorganism.[12] Furthermore, a variety of tripodal hydroxamate ligands have been synthesized as ferrichrome models[17] and their biological activities investigated.[18] Moreover, potential applications have been attempted with certain trihydroxamates, for example, in supramolecular chemistry.[19−22]

Although there have been extensive studies of iron(III) complexation with monotopic hydroxamate ligands,[11,23,24] only limited information is available about multitopic iron complexation.[19,21] Dihydroxamic acids, represented by siderophore rhodotorulic acid, are known to form binuclear iron complexes,[25] but their manner of fragmentary decomplexation makes them unsuitable for iron-storage experiments.[26,27]

We have synthesized a number of amino acid- and peptide-based monotopic hydroxamate ligands to study iron complexation.[28−31] Multitopic hydroxamate ligands can be synthesized by the extension of the framework of these monotopic ligands. Ditopic ligands, for example, present an interesting problem of iron mobilization within a ligand. It is important to study this for obtaining information related to intracellular iron migration behavior which is not yet understood well.[1] We describe here the synthesis of tripodal monotopic and ditopic hydroxamate ligands (**1** and **2**) and the formation and kinetic and thermodynamic properties of their metal-ion complexes. The results are compared to those reported for linear and cyclic ligands **3** and **4**[28] (Chart 1). In related studies, Shanzer's group has reported tripodal, ditopic hydroxamate ligands (for example, **5** in Chart 1) and observed the iron complex formation of a "triple-helical" structure;[19,21] however, further iron-mobilization studies remain to be done.

Chart 1

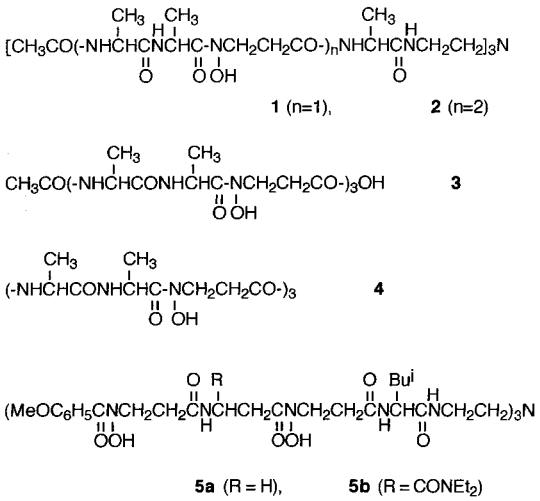

To explore the potential of ditopic ligands for an iron reservoir model, we performed iron-loading and -removal reactions using even M(III)-preloaded ligands, a study that should help to elucidate incoming Fe(III) behavior when in competition with M(III), but which has rarely been carried out.[32,33] The group-13 M(III) ions (M = Al, Ga, and In) are used as surrogates of Fe(III). They are diamagnetic and have similar charge/radius ratios, produce similar octahedral complexes, and exhibit different affinities for given ligands.[15,34−36] It is also convenient that their hydroxamato complexes do not absorb in the visible region.

Iron(III) complexes of **1** and **2** were prepared by pH-dependent transformation from bis(hydroxamato)iron to tris(hydroxamato)iron complexes. The latter were characterized by UV−vis and CD spectroscopy, along with ESIMS. Tris complexes were also formed by iron loading on ligands or on M(III)-preloaded ligands using ammonium ferric oxalate as a soluble and exchangeable iron source at near-neutral pH. The iron-removal reaction of the complexes of **2** with excess EDTA allowed us to characterize the iron-bound states and distributions. With the ligand protonation constants and the iron(III) complex stability constants obtained, we discuss briefly a model for biological iron mobilization.

Results

Hydroxamate Ligands. Tris(alanylaminoethyl)amine[31] was combined with a peptide strand containing one or two hydroxamate groups to anchor three strands together. Scheme 1

(14) van der Helm, D.; Baker, J. R.; Eng-Wilmont, D. L.; Hossain, M. B.; Loghry, R. A. *J. Am. Chem. Soc.* **1980**, *102*, 4224−4231.
(15) (a) Llinás, M.; Klein, P. M.; Neilands, J. B. *J. Mol. Biol*. **1970**, *52*, 399−414. (b) Llinás, M.; Klein, P. M.; Neilands, J. B. *J. Mol. Biol*. **1972**, *68*, 265−284.
(16) Tufano, T. P.; Raymond, K. N. *J. Am. Chem. Soc*. **1981**, *103*, 6617−6624.
(17) (a) Naegeli, H.-U.; Keller-Schierlein, W. *Helv. Chim. Acta* **1978**, *61*, 2088−2095. (b) Olsen, R. K.; Ramasamy, K. *J. Org. Chem*. **1985**, *50*, 2264−2271. (c) Akiyama, M.; Katoh, A.; Mutoh, T. *J. Org. Chem*. **1988**, *53*, 6089−6094.
(18) (a) Lee, B. H.; Miller, M. J. Prody, C. A.; Neilands, J. B. *J. Med. Chem*. **1985**, *28*, 317−323, 323−327. (b) Tor, Y.; Libman, J.; Shanzer, A. *J. Am. Chem. Soc*. **1987**, *109*, 6518−6519. (c) Ng, C. Y.; Rodgers, S. J.; Raymond, K. N. *Inorg. Chem*. **1989**, *28*, 2062−2066. (d) Katoh, A.; Akiyama, M. *J. Chem. Soc., Perkin Trans. 1* **1991**, 1839−1842. (e) Dayan, I.; Libman, J.; Agi, Y.; Shanzer, A. *Inorg. Chem*. **1993**, *32*, 1467−1475. (f) Esteves, M. A.; Vaz, M. C. T.; Gonçalves, M. L. S. S.; Farkas, E.; Santos, M. A. *J. Chem. Soc., Dalton Trans*. **1995**, 2565−2573. (g) Ramurthy, S.; Miller, M. J. *J. Org. Chem*. **1996**, *61*, 4120−4124.
(19) Libman, J.; Tor, Y.; Shanzer, A. *J. Am. Chem. Soc*. **1987**, *109*, 5880−5881.
(20) Spasojević, I.; Batinić-Haberle, I.; Choo, P. L.; Crumbliss, A. L. *J. Am. Chem. Soc*. **1994**, *116*, 5714−5721.
(21) Blanc, S.; Yakirevitch, P.; Leize, E.; Meyer, M.; Libman, J.; Van Dorsselaer, A.; Albrecht-Gary, A.-M.; Shanzer, A. *J. Am. Chem. Soc*. **1997**, *119*, 4934−4944.
(22) Akiyama, M.; Katoh, A.; Kato, J.; Takahashi, K.; Hattori, K. *Chem. Lett*. **1991**, 1189−1192.
(23) (a) Crumbliss, A. L. In *Handbook of Microbial Iron Chelates*; Winkelmann, G., Ed.; CRC Press: Boca Raton, FL, 1991; pp 177−233. (b) Albrecht-Gary, A.-M.; Crumbliss, A. L. In *Metal Ions in Biological Systems*; Sigel, A., Sigel, H., Eds.; Marcel Dekker: New York, 1998; Vol. 35, pp 239−328.
(24) Biruš, M.; Kujundžic, N.; Pribanić, M. *Prog. React. Kinet.* **1993**, *18*, 171−271.
(25) Carrano, C. J.; Raymond, K. N. *J. Am. Chem. Soc*. **1978**, *100*, 537−5374.
(26) Barclay, S. J.; Huynh, B. H.; Raymond, K. N. *Inorg. Chem*. **1984**, *23*, 2011−2018.
(27) (a) Caudle, M. T.; Cogswell, L. P., III; Crumbliss, A. L. *Inorg. Chem*. **1994**, *33*, 4759−4773. (b) Spasojević, I.; Boukhalfa, H.; Stevens, R. D.; Crumbliss, A. L. *Inorg. Chem*. **2001**, *40*, 49−58.
(28) Hara, Y.; Akiyama, M. *Inorg. Chem.* **1996**, *35*, 5173−5180.
(29) (a) Shimizu, K.; Hasegawa, M.; Akiyama, M. *Bull. Chem. Soc. Jpn*. **1984**, *57*, 495−499. (b) Akiyama, M.; Katoh, A.; Iijima, M.; Takagi, T.; Natori, K.; Kojima, T. *Bull. Chem. Soc. Jpn*. **1992**, *65*, 1356−1361. (c) Akiyama, M.; Katoh, A.; Mutsui, Y.; Watanabe, Y.; Umemoto, K. *Chem. Lett.* **1996**, 915−916.
(30) Shimizu, K.; Akiyama, M. *J. Chem. Soc., Chem. Commun.* **1985**, 183−184.
(31) Akiyama, M.; Hara, Y.; Gunji, H. *Chem. Lett.* **1995**, 225−226.
(32) Biruš, M.; Bradić, Z.; Krznarić, G.; Kujundžic, N.; Pribanić, M.; Wilkins, P. C.; Wilkins, R. G. *Inorg. Chem*. **1987**, *26*, 1000−1005.
(33) Ga(III) in Ga−deferriferrichrome A was replaced by the use of a large excess of Fe(III)−nitrilotriacetate; Emery, T.; Hoffer, P. B. *J. Nucl. Med*. **1980**, *21*, 935−939.
(34) Anderegg, G.; L'Eplattenier, F.; Schwarzenbach, G. *Helv. Chim. Acta* **1963**, *46*, 1400−1408, 1409−1422.
(35) Borgias, B.; Hugi, A. D.; Raymond, K. N. *Inorg. Chem*. **1989**, *28*, 3538−3545.
(36) Evers, A.; Hancock, R. D.; Martell, A. E.; Motekaitis, R. J. *Inorg. Chem*. **1989**, *28*, 2189−2195.

Scheme 1[a]

Boc-Ala-Ala-β(BnO)Ala-OH (**6a**) + (TFA·H-Ala-NHCH$_2$CH$_2$)$_3$N (**7b**)

$\xrightarrow{\text{i}}$ {X-Ala-Ala-β(YO)Ala-Ala-NHCH$_2$CH$_2$]$_3$N (**8a**) (X=Boc, Y=Bn)

8a $\xrightarrow{\text{ii}}$ **8b** (X=H, Y=Bn) $\xrightarrow{\text{iii}}$ **8c** (X=Ac, Y=Bn) $\xrightarrow{\text{iv}}$ **1**

6a + **8b** $\xrightarrow{\text{v}}$ {X-[Ala-Ala-β(YO)Ala-]$_2$Ala-NHCH$_2$CH$_2$}$_3$N (**9a**) (X=Boc, Y=Bn)

9a $\xrightarrow{\text{ii}}$ **9b** (X=H, Y=Bn) $\xrightarrow{\text{iii}}$ **9c** (X=Ac, Y=Bn) $\xrightarrow{\text{iv}}$ **2**

[a] Reagents and conditions: i. EDC, HOBt, NMM, −10 °C; ii, TFA in CH_2Cl_2, 0 °C; iii, AcONSu, NMM, −10 °C; iv, H_2, 10% Pd/C in MeOH; v, BOP reagent, HOBt, Et_3N, 0 °C.

summarizes the synthesis of ligands **1** and **2**.[37] The protected form of **1** was synthesized with a Boc-Ala-Ala-β-(BnO)Ala-OH unit,[28] and the protected form of **2** was derived from this form by use of the same unit. Ligands **1** and **2** were obtained by deprotection and characterized by IR, ^{1}H NMR, and elemental analysis. They were soluble in DMF, DMSO, and water, but not in $CHCl_3$ or acetonitrile.

Data for the ^{1}H NMR spectra of **1** and **2** in DMSO-d_6 solutions are presented (Table S1). The spectral patterns of **1** and **2** suggest C_3 symmetry of the molecules, and individual signals were assigned using 2D COSY−NOESY techniques. Each amino acid residue in the ligands and the Ga(III) complexes (vide infra) is numbered as follows:

1: [Ac-Ala^1-Ala^2-β-(HO)Ala-Ala^3-NHCH$_2$CH$_2$]$_3$N

2: [Ac-Ala^1-Ala^2-β-(HO)Ala^1-Ala^3-Ala^4-β-(HO)Ala^2-Ala^5-NHCH$_2$CH$_2$]$_3$N

In particular, the α-protons of Ala^2 of **1** and of Ala^2 and Ala^4 of **2** appeared at about 4.80 ppm with full intensity of 3H and 6H, respectively, which confirmed the presence of the hydroxamic acid groups. The temperature coefficients of amide-proton chemical shifts were found to be in the range of -4 to -5×10^{-3} ppm deg^{-1}. These are more negative than the value (-3×10^{-3} ppm deg^{-1}) for intramolecularly hydrogen-bonded amide-protons.[15a,38]

Iron(III) Complexes. Iron(III) complex formation of hydroxamate groups is expressed as a series of pH-dependent equilibrium processes (eq 1),[39−41] where Fe^{3+} represents an aqua iron species and H_3L stands for an iron binding site of three hydroxamate groups. The symbol H_3L-H_3L is used for **2**.

$$Fe^{3+} + H_3L \rightleftharpoons Fe(H_2L)^{2+} + H^+ \rightleftharpoons Fe(HL)^+ + 2H^+ \rightleftharpoons Fe(L) + 3H^+ \quad (1)$$

A ferric nitrate solution (1 equiv or 1 or 2 equiv, respectively) was mixed with **1** or **2**, producing an acidic solution which contained essentially bis(hydroxamato)iron(III) species, Fe-

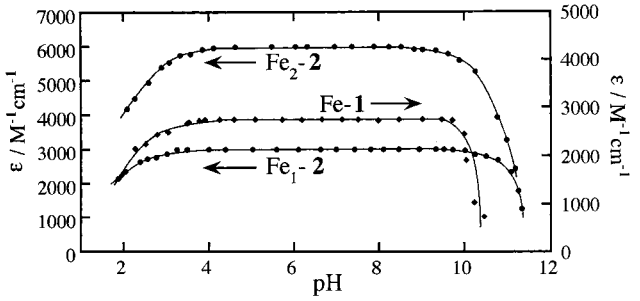

Figure 1. Absorption (ϵ/M^{-1} cm^{-1}) at 425 nm vs pH in water at 25 °C.

(HL)$^+$,[39,42] with λ_{max} at 465 nm. The Fe(HL)$^+$ complexes were transformed to tris(hydroxamato)iron(III) complexes, Fe(L), by neutralization to pH 7: Fe(L) for **1**, and Fe(L-H_3L) and Fe$_2$(L-L) for **2**, each of which is designated as Fe-**1**, Fe$_1$-**2**, or Fe$_2$-**2**, respectively. Their UV−vis spectra showed λ_{max} at 425 nm with values of ϵ 2800 for Fe-**1** and 3000 M^{-1} cm^{-1}/Fe(III) for Fe$_1$-**2** and Fe$_2$-**2**, typical of Fe(L) complexes.[34] Iron in Fe$_1$-**2** resides mostly (93%) at a near tren site of **2** (see Table 3, entry 4b).

Plots of the absorbance at 425 nm versus pH shown in Figure 1 exhibit a plateau region, where iron(III) exists essentially as Fe(L). When an Fe(L) solution was gradually acidified, the absorption maximum shifted to the red, and its intensity decreased.[39] Isosbestic points were observed for Fe-**1** at 447 nm, and for Fe$_1$-**2** and Fe$_2$-**2** at 465 nm, respectively, which indicate an equilibrium reaction occurring between Fe(L) and Fe(HL)$^+$ (eq 2). With Fe$_2$-**2**, only two species, Fe$_2$(L-L) and Fe$_2$(HL-L)$^+$, are present in the pH range of 3.1−4.0, judged from the magnitude of absorbance.

$$Fe(L) + H^+ \rightleftharpoons Fe(HL)^+, K_{Fe(HL)} = [Fe(HL)^+]/[Fe(L)][H^+] \quad (2)$$

$$A_{obs} = (A_{Fe(L)} - A_{obs})/K_{Fe(HL)}[H^+] + \epsilon_{Fe(HL)}c_t \quad (3)$$

The spectral data was analyzed using Schwarzenbach plot (eq 3),[39] as shown for the case of Fe$_2$-**2** (Figure 2), and the $K_{Fe(HL)}$ values obtained are listed in Table 4.

Gallium(III) Complexes. Ga$_1$-**2** exhibited an ^{1}H NMR spectral pattern of C_3 symmetry (Table S1). The signals of α-CH Ala^4 shifted 0.12 ppm downfield and of NH Ala^5 0.17 ppm downfield, relative to those protons of **2**. Likewise, the signals of NH Ala^4 shifted 0.04 ppm upfield and of α-CH Ala^5 0.04 ppm upfield. These protons exhibited cross-peaks with the NH and β-CH$_2$ protons of the tren moiety by COSY−NOSEY measurements. The Ga location in Ga$_1$-**2** was assigned to a nearby tren site, namely, the lower binding site. The NH and α-CH protons of Ala^1, Ala^2, and Ala^3 residues appear little shifted.

The spectral pattern of Ga-**1** was also C_3-symmetric. Its signals for α-CH Ala^2 and NH Ala^3 shifted 0.11 and 0.14 ppm downfield, relative to the corresponding protons of **1**. This shift pattern for Ga-**1** is similar to that observed for Ga$_1$-**2**, supporting the assignment of the location of Ga(III) in **2**.

CD Spectra of Iron Complexes. Cotton effects at 365 and 450 nm were observed for the iron(III) complexes of **1** and **2** (Table 1), and the Δ configuration around the iron center was assigned to them by comparison with the structure of ferrichrome, together with the *cis* configuration by using NMR data which indicated C_3 symmetric structures.[13,14] Notable

(37) Abbreviations are as follows: Ala, L-alanine; β-(HO)Ala or β-(BnO)-Ala, *N*-hydroxy- or *N*-(benzyloxy)-β-alanine; Boc, *tert*-butyloxycarbonyl; BOP, (benzotriazol-1-yloxy)tris(dimethylamino)phosphonium hexafluorophosphate(V); EDC, 1-ethyl-3-[(3-dimethylamino)propyl]carbodiimide; EDTA, ethylenediaminetetraacetic acid; HOBt, 1-hydroxybenzotriazole; NMM, *N*-methylmorpholine; TFA, trifluoroacetic acid; tren, tris(aminoethyl)amine; AcOSu, *N*-acetoxysuccinimide; THF, tetrahydrofuran; DMSO, dimethyl sulfoxide.

(38) Ohnishi, M.; Urry, D. W. *Biochem. Biophys. Res. Commun.* **1967**, *36*, 194−202.

(39) Schwarzenbach, G.; Schwarzenbach, K. *Helv. Chim. Acta* **1963**, *46*, 1390−1400.

(40) Monzyk, B.; Crumbliss, A. L. *J. Am. Chem. Soc.* **1979**, *101*, 6203−6213.

(41) Biruš, M.; Bradić, Z.; Kujundžic, N.; Pribanić, M.; Wilkins, P. C.; Wilkins, R. G. *Inorg. Chem.* **1985**, *24*, 3980−3983.

(42) Caudle, M. T.; Stevens, R. D.; Crumbliss, A. L. *Inorg. Chem.* **1994**, *33*, 843−844, 6111−6115.

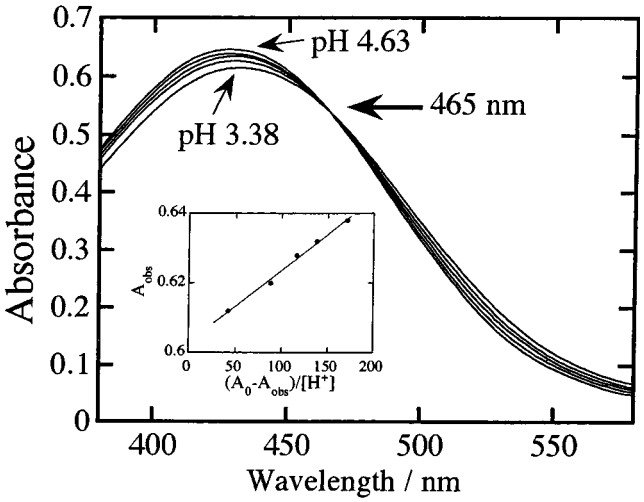

Figure 2. UV−vis spectra of Fe_2-**2** showing an isosbestic point. The concentrations of [ligand] and [Fe(III)] are 1.1×10^{-4} M and 2.2×10^{-4} M, respectively, in water at 25 °C. The insert is a Schwarzenbach plot for the spectral data.

Table 1. Summary of CD Spectral Data[a]

Fe(III) complex	band/nm ($\Delta\epsilon$)		type	ref
Fe-**1**	365 (+2.3)	445 (−4.0)	Δ	
Fe_1-**2**	365 (+2.9)	450 (−6.3)	Δ	
Fe_2-**2**	365 (+5.9)	450 (−12.0)	Δ	
FeAl-**2**[b]	365 (+2.7)	450 (−5.8)	Δ	
FeGa-**2**[b]	365 (+2.3)	450 (−5.9)	Δ	
FeIn-**2**[b]	365 (+2.8)	450 (−5.3)	Δ	
Fe-**3**	360 (+3.0)	445 (−7.5)	Δ	28
Fe-**4**	360 (+4.4)	445 (−6.8)	Δ	28
Fe_1-**5**	380 (+1.3)	445 (−0.76)	Δ	21
Fe_2-**5**	375 (+5.1)	460 (−2.6)	Δ	21
ferrichrome	360 (−3.7)	465 (+2.4)	Λ	14

[a] Determined in water at 25 °C and pH 7.0. [b] Prepared by 1-equiv iron loading on M_1-**2**, where M = Al, Ga, or In; Fe(III) resides mostly (75%−79%) at the lower site: See Table 3 for the data.

features are as follows. (1) The CD intensity (from the top of the peak to the bottom of the trough) of Fe_1-**2** is comparable to that of Fe-**3** or Fe-**4**, and higher than that of Fe-**1**, the latter being comparable to ferrichrome.[14] (2) The intensity of Fe_2-**2** is quite high, almost twice as high as that of Fe_1-**2**. (3) Complexes Fe_1-**2** and Fe_2-**2** exhibited higher CD intensity than those of previously reported complexes, for example, Fe_1-**5** and Fe_2-**5**.[19,21]

Iron Loading with Ferric Oxalate. Initially, the loading process directly from a ligand (eq 4a) or from an M(III)-preloaded ligand, M(L), (eq 4b) was investigated using ammonium tris(oxalato)iron(III). The reactions are as outlined below, which show the processes from H_3L and M(L) via mono- and bis(hydroxamato) complexes to the tris(hydroxamato)iron(III) complex, Fe(L),[16,23,39] with the final production of $3HC_2O_4^-$ (4a) and $M(C_2O_4)_3^{3-}$ (4b), respectively.

$$H_3L + Fe(C_2O_4)_3^{3-} \rightleftharpoons (H_2L)Fe(C_2O_4)_2^{2-} + HC_2O_4^- \rightleftharpoons (HL)F(C_2O_4)_1^- + 2HC_2O_4^- \rightleftharpoons Fe(L) + 3HC_2O_4^- \quad (4a)$$

where H_3L stands for an iron binding site in **1** and **2**.

$$M(L) + Fe(C_2O_4)_3^{3-} \rightleftharpoons (C_2O_4)^-M(L)Fe(C_2O_4)_2^{2-} \rightleftharpoons (C_2O_4)_2^{2-}M(L)F(C_2O_4)^- \rightleftharpoons Fe(L) + M(C_2O_4)_3^{3-} \quad (4b)$$

where M(L) represents an M(III) ion residing in **1** and **2**.

Table 2. Iron(III) Loading with Tris(oxalato)Iron(III) Complex[a]

		apparent second-order rate constant ($k_{2\,app}$/M^{-1} s^{-1})		
			2-equiv loading[c]	
entry	ligand	1-equiv[b] loading	first iron	second iron
1a	**1**	1.7×10^3[d]		
1b	**2**	1.4×10^3	1.0×10^3	1.0×10^3
1c	Fe_1-**2**	1.1×10^3[e]		
2a	Al-**1**	1.8×10^2		
2b	Ga-**1**	5.4×10^2		
2c	In-**1**	3.4×10^3		
3a	Al_1-**2**	1.1×10^2	2.1×10^2	1.5×10
3b	Ga_1-**2**	2.6×10^2	2.3×10^2	8.1×10
3c	In_1-**2**	4.3×10^3	3.3×10^3	3.3×10^3

[a] Iron(III) was loaded in aqueous acetate buffer at 25.0 ± 0.1 °C, pH 5.4, and ionic strength 0.10 (KCl), using ammonium ferric oxalate. [b] The initial concentration of [ligand] and [Fe(III)] = 6.5×10^{-5} M. Experimental errors are estimated to be ±10%, except for faster reactions ($k_{2\,app}$/M^{-1} $s^{-1} \approx 10^3$), in which they are ±20%. [c] For 2-equiv loading, [ligand] = 6.5×10^{-5} M and [Fe(III)] = 1.3×10^{-4} M. [d] A similar value was obtained with 0.10 M $K(NO_3)$. [e] Data were obtained by the second 1-equiv loading after completion of the first 1-equiv reaction.

The increase in absorbance of Fe(L) at 425 nm was monitored in an aqueous acetate buffer at 25 °C and pH 5.4. With 1 and 2 equiv of ferric oxalate, ligands **1**, M-**1**, or M_1-**2** and **2** or M_1-**2** were cleanly transformed to Fe-**1** or FeM-**2** and Fe_2-**2**, respectively, in a matter of minutes, as evidenced by UV−vis spectra. For the purpose of comparison, the rates of formation of Fe-**1**, FeM-**2**, and Fe_2-**2** were followed, and the second-order rate constants with respect to the ferric oxalate and either a free ligand or a M(III)-preloaded ligand,[43] as expressed by eq 5, were obtained.[44] Table 2 summarizes these rate constants.[45]

$$\text{rate} = k_{2\,app}[Fe(C_2O_4)_3^{3-}][H_3L, \text{ or } M(L)] \quad (5)$$

Absorbance changes versus time for 2-equiv loading on **2** and M_1-**2** are shown in Figure 3 A, with second-order rate plots in the insert. Shown in Figure 3 B are absorbance changes in the early stages of 1- and 2-equiv iron loading, emphasizing different rates for different-M(III) preloaded ligands (each portion is depicted in a different time scale).

The $k_{2\,app}$ values are different and increase in the order Al-**1** < Ga-**1** < In-**1** with factors of 3 and then 6 based on the rate of Al-**1**, and Al_1-**2** < Ga_1-**2** < Fe_1-**2** < In_1-**2** with factors of 2.5, 4, and 4 based on the rate of Al_1-**2**, respectively.

Characterization of FeM-**2** complexes was made by CD spectroscopy (Table 1), ESIMS, and UV−vis spectra; the last spectra were the same as that of Fe_1-**2**.

Electrospray Ionization Mass Spectrometry. The spectra of Fe_2-**2** showed peaks due to tri-, di-, and monocation species, and the spectra of FeAl-**2** and FeGa-**2** exhibited dication peaks. With In_1-**2**, however, peaks were assignable to the ligand, but not to In_1-**2**. Under these conditions, small peaks ascribable to FeIn-**2** were detected in the spectra recorded on the + or − voltage mode. Unlike the previous ditopic case,[21] fragmentation peaks of M-16 that arise from the deoxygenated hydroxamate moiety were not detected.

(43) Wilkins, R. G. *Kinetics and Mechanism of Reactions of Transition Metal Complexes*, 2nd ed.; VCH: Weinheim, 1991.

(44) The second-order reactions are among the most commonly encountered ones (ref 43, pp 24 and 68−69).

(45) The rate constants for slow second phases were obtained from the slopes of the plots. The progress of reaction in individual cases showed a pattern which is very similar to that illustrated in Figure 3A for 2-equiv loading on In_1-**2**.

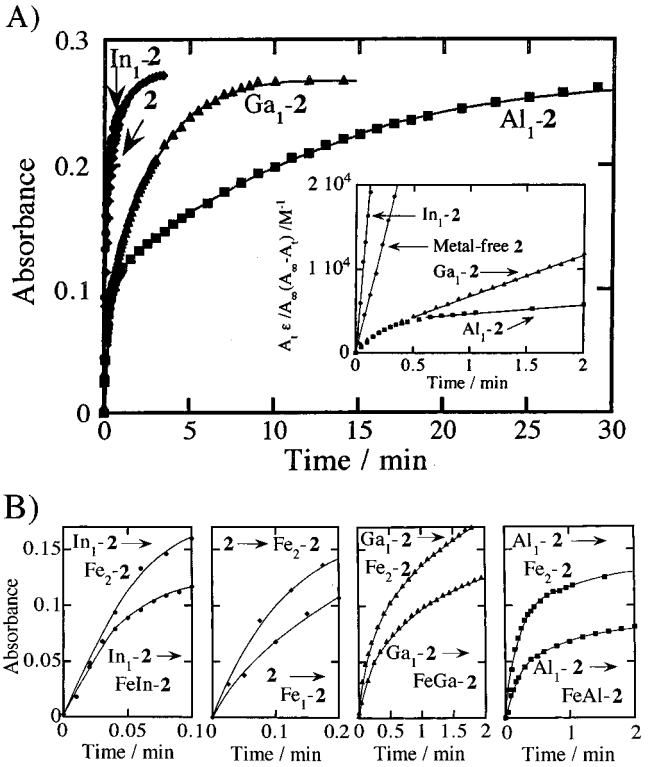

Figure 3. (A) Plots of absorbance at 425 nm vs time for 2-equiv iron loading on **2** and on M_1-**2** which produces Fe_2-**2**. The insert shows second-order rate plots for the 2-equiv loading. The same rate throughout the reaction is seen for **2** and In_1-**2**, while a break is noted for Al_1-**2** or Ga_1-**2** at the 1-equiv loaded stage, and the corresponding rate constants are obtained from that slope. (B) Absorbance changes vs time at the early stages for loading of both 1- and 2-equiv cases. Note the different time scales.

Iron Removal Rates. Subsequently, the metal-bound states of the formed complexes were examined by the measurement of iron-removal rates with EDTA. The removal reaction is of a ligand-exchange type and proceeds through the proton-assisted formation of a ternary complex of a ligand, Fe(III), and EDTA and its subsequent breakdown into products, the ligand and $Fe(EDTA)^-$ (eq 6), as discussed by Tufano and Raymond and later Albrecht-Gary et al.[16,46]

$$\mathrm{Fe(L)} + \mathrm{H^+} \rightleftharpoons \mathrm{Fe(HL)^+}$$

$$\mathrm{Fe(HL)^+} + \mathrm{H_2EDTA^{2-}} \rightleftharpoons \mathrm{(HL)Fe(H_2EDTA)^-} \rightleftharpoons \mathrm{H_3L} + \mathrm{Fe(EDTA)^-} \quad (6)$$

A decrease in absorbance of Fe(L) at 425 nm was monitored under pseudo-first-order conditions with a 20 M excess of EDTA at pH 5.4 and 25 °C;[16,28,46] the data sets of absorbance change with respect to time were collected and analyzed using the models described below.

(i) Reaction Models. Four models of first-order kinetics are used, depending on the types of complexes: a monotopic complex, Fe-**1** (case 1); a fully loaded ditopic complex, Fe_2-**2** (case 2); a half-loaded ditopic complex, Fe_1-**2** (case 3); and mixed binuclear complexes, FeM-**2** (case 4).

For case 1 (Fe-**1**), the pseudo-first-order kinetic equation is used.

(46) Albrecht-Gary, A.-M.; Palanche-Passeron, T.; Rochel, N.; Hennard, C.; Abdallah, M. A. *New J. Chem.* **1995**, *19*, 105−113.

Scheme 2

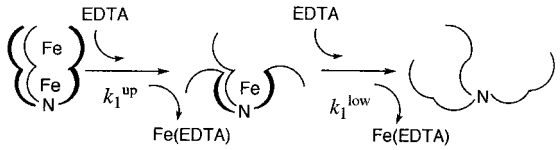

For the analysis of cases 2 and 4, consecutive first-order kinetic equations are applied.[43] In case 2 (Fe_2-**2**), iron at the upper site is disposed of, but iron at the lower site can only be removed after the upper site. This situation is analyzed by applying a consecutive first-order kinetic model, and the overall removal process can be described by pseudo-first-order rate constants for the ferric ions at the upper site and the lower site, k_1^{up} and k_1^{low} (Scheme 2). The absorbance (A_t) at time t for the species in the reaction mixture is expressed by eq 7. The two binding sites have equal ϵ values, and the contribution of $Fe(EDTA)^-$ can be neglected for most of the reaction.

$$A_t = \text{absorbance of the reaction mixture composed of } \mathrm{Fe_2}\text{-}\mathbf{2}, \mathrm{Fe_1}\text{-}\mathbf{2}, \text{ and } \mathrm{Fe(EDTA)^-} = A_0 \exp(-k_1^{up} t) + {}^1/_2 A_0 \{k_1^{up}/(k_1^{up} - k_1^{low})\}\{\exp(-k_1^{low} t) - \exp(-k_1^{up} t)\} \quad (7)$$

In case 3 (Fe_1-**2**), iron may reside partly at the lower site and partly at the upper site, and the extent of reaction is expressed by a parallel first-order rate law (eq 8).[43] This equation also uses the rate constants k_1^{up} and k_1^{low}, with iron-residing probability (P) at the lower site.

$$\text{Extent of reaction } (A_t/A_0) = P \exp(-k_1^{low} t) + (1 - P) \exp(-k_1^{up} t) \quad (8)$$

For analysis of case 4 (FeM-**2**), we modify eq 7 to evaluate a contribution from M(III) ion (M = Al, Ga, and In), and eq 9 is derived, in which P refers to the lower site. The rate constant k_1^{up-M} for M(III) at the upper site is obtained in the process of the curve fit, but the rate constant k_1^{low-M} is not evaluated.

$$A_t/A_0 = (1 - P) \exp(-k_1^{up} t) + {}^1/_2 P\{k_1^{up-M}/(k_1^{up-M} - k_1^{low})\}\{\exp(-k_1^{low} t) - \exp(-k_1^{up-M} t)\} \quad (9)$$

(ii) Reaction Rates. The pseudo-first-order rate constant was determined to be 2.7×10^{-2} s^{-1} for Fe-**1** (a corresponding second-order rate constant is calculated to be 10.4 M^{-1} s^{-1}) in the presence of EDTA (2.6×10^{-3} M). This rate is comparable to the rate of 1.8×10^{-2} s^{-1} reported for Fe-**3**.[28]

In each of the cases 2−4, one of the equations of 7, 8, and 9 was used to generate curve fits for the plotted absorbance change with respect to time, and each rate constant was obtained. An excellent fit between experimental data (absorbance changes vs time) and a calculated curve based on given k_1^{up} and k_1^{low} values is shown for the Fe_2-**2** reaction (Figure 4), where the three calculated curves for Fe_2-**2**, intermediate monoferric Fe_1-**2**, and the total reaction mixture represent the progress of the reaction. Table 3 lists the kinetic data and the iron distribution probability. Allowable deviations in all cases were small; they were determined by the same curve-fit, applying slightly different values of k_1^{up}, k_1^{low}, or P.

Furthermore, we carried out iron-removal reactions for Fe_2-**2** using different EDTA concentrations and observed a hyperbolic dependence of both k_1^{up} and k_1^{low} on the EDTA concentration (Figure 5). In this case the kinetic data was applied to a modification of eq 6 for simplicity, as the back reaction from

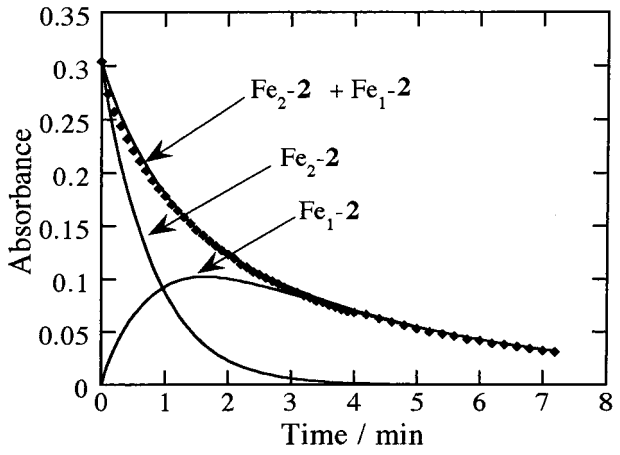

Figure 4. A typical curve for absorbance (at 425 nm) changes vs time for iron removal (here from Fe_2-**2**) by EDTA. The rate constants k_1^{up} and k_1^{low} were obtained from a best fit (bold line) of the experimental data (dots) to eq 7. The iron at the upper site is removed by the k_1^{up} constant (solid line), while the iron at the lower site is once "exposed" and removed by the k_1^{low} constant (solid line).

Table 3. Pseudo-First-Order Rate Constants for Displacement of Iron(III) from Monotopic and Ditopic Complexes and Iron(III) Residence Percentages[a]

entry	metal ion complex[b]	upper site $10^2k_1^{up}/s^{-1}$ (mol %)[c]	lower site $10^3k_1^{low}/s^{-1}$ (mol %)[c]	upper site $10k_1^{up-M}/s^{-1}$ for M(III)[upd]
4a	Fe_2-**2**	2.1 ± 0.1	4.0 ± 0.2	
4b	Fe_1-**2**[e]	1.7 ± 0.2 (7 ± 3)	3.8 ± 0.2 (93 ± 3)	
5a	FeAl-**2**	2.2 ± 0.4 (25 ± 5)	4.2 ± 0.2 (75 ± 5)	1.4 ± 0.4
5b	FeGa-**2**	3.0 ± 0.3 (21 ± 3)	3.9 ± 0.2 (79 ± 3)	1.2 ± 0.3
5c	FeIn-**2**	3 ± 1 (25 ± 5)	4.2 ± 0.2 (75 ± 5)	6 ± 1

[a] In an acetate buffer at 25 ± 0.1 °C and pH 5.4, with 20 M excess of EDTA (1.3×10^{-3} M), at ionic strength (KCl) = 0.1. [Fe_1-**2**], [Fe_2-**2**], or [FeM-**2**] = 6.5×10^{-5} M. Allowable deviations for both rate constants and distribution percentages were determined through the curve fits and are given by digits with ± sign. [b] FeM-**2**, where M = Al, Ga, or In, denotes a dinuclear complex. [c] Iron residence percentage was determined by curve fit of the kinetic data to eq 8 or 9 (see text). [d] $M(III)^{up}$ removal rate was obtained by curve fit to eq 9, and M(III) residence percentage was taken as the same that for the lower-site iron. [e] In another run, values obtained were $10^2k_1^{up}/s^{-1} = 2.2 \pm 0.2$ with (6 ± 3) mol % for the upper site, and $10^3k_1^{low}/s^{-1} = 3.6 \pm 0.2$ with (94 ± 3) mol % for the lower site.

the product to the intermediate ternary complex is negligible, as reported by others and by us.[16,46,47] In this way, the formation constant of the intermediate ternary complex, K_{int}, and the maximal first-order rate constant for breakdown of the intermediate into products, k_{max}, were determined to be 0.79 mM^{-1} and 4.5×10^{-2} s^{-1} for the upper site and 0.72 mM^{-1} and 8.8×10^{-3} s^{-1} for the lower site.

Protonation and Stability Constants. The proton dissociation equilibrium and its protonation constants are defined by eq 10 for the hydroxamic acid groups of ligands **1** and **2**, where $n = 1$, 2, and 3 for **1**, and $n = 1$, 2, ..., 6 for **2**.

$$H_{n-1}L + H^+ \rightleftharpoons H_nL,\ K_n = [H_nL]/[H^+][H_{n-1}L] \quad (10)$$

Potentiometric titration was carried out in water at 25.0 ± 0.1 °C; the constants (p*K*) obtained are 9.69, 9.03, and 8.26 for **1**, and 9.52, 9.39, 9.02, 8.76, 8.46, and 7.81 for **2**. Six p*K* values for **2** lie in a narrow range of only 1.7 p*K* units, and the average hydroxamate pK_{av} values for **1** and **2** are smaller than that of **3** and **4** (Table 4).

(47) Hara, Y.; Shen, L.; Tsubouchi, A.; Akiyama, M.; Umemoto, K. *Inorg. Chem.* **2000**, *39*, 5074−5082.

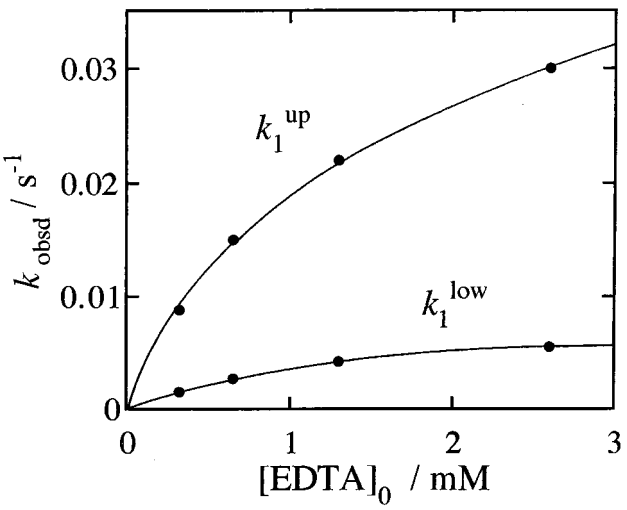

Figure 5. Hyperbolic dependence of the rates of iron removal from the upper site and lower site of Fe_2-**2** upon EDTA concentration.

Table 4. Average Ligand Protonation Constants and the ϵ Values, Monoprotonation Constants, and Stability Constants of Iron(III) Complexes[a]

Fe complex	Fe-**1**	Fe_1-**2**	Fe_2-**2**	Fe-**3**[b]	Fe-**4**[b]	ferrichrome[c]
pK_{av}[d]	8.99	8.82	9.14	9.14	8.98	
$\epsilon/M^{-1}\,cm^{-1}$	2800	3000	6000	2890	2830	2890
$K_{Fe(HL)} \times 10^{-3}$	0.926	1.33	5.01	1.44	2.24×10^3	0.031
$\log K_{Fe(L)}$	28.2	28.5[e]	29.0[f]	27.4	28.3	29.1

[a] In water at 25.0 ± 0.1 °C with ionic strength 0.10 (KCl). The equilibrium exchange reaction was performed using an equimolar amount of EDTA (1.3×10^{-4} M): Fe_1-**2** remained 22% (eq 12a) and $K_{eq1} = 3.82 \times 10^6$; Fe_2-**2** remained 35% (eq 12b) and $K_{eq2} = 1.01 \times 10^6$. [b] Reference 28. [c] References 14 and 34. [d] The protonation constant of the tertiary nitrogen (pK_N), 5.68 for **1** and 5.35 for **2**. [e] Value corresponds to the lower site of **2**. [f] Value stands for the upper site of **2**.

It is difficult to experimentally perform an equilibrium reaction involving only the two species, H_3L-H_3L and Fe_2(L-L), because the transformation inevitably involves the intervening monoferric complex, Fe(L-H_3L). The proton-independent stability constants for Fe_2-**2**, therefore, are described by eqs 11a and 11b. The equation for Fe-**1** is omitted to avoid duplication of monotopic complexation.

$$Fe^{3+} + H_3L\text{-}L^{3-} \rightleftharpoons Fe(L\text{-}H_3L),\quad K_{Fe(L-H_3L)} = [Fe(L\text{-}H_3L)]/[Fe^{3+}][H_3L\text{-}L^{3-}] \quad (11a)$$

$$Fe^{3+} + Fe(L\text{-}L)^{3-} \rightleftharpoons Fe_2(L\text{-}L),\quad K_{Fe_2(L-L)} = [Fe_2(L\text{-}L)]/[Fe^{3+}][Fe(L\text{-}L)^{3-}] \quad (11b)$$

We carried out the ligand-exchange reactions given by eqs 12a and 12b, using equimolar amounts of Fe_1-**2** and H_2EDTA^{2-}, and of Fe_2-**2** and H_2EDTA^{2-}, respectively, at 25.0 ± 0.1 °C, ionic strength 0.10, and pH 7.0.

$$Fe(L\text{-}H_3L) + H_2EDTA^{2-} + H^+ \rightleftharpoons Fe(EDTA)^- + H_3L\text{-}H_3L \quad (12a)$$

$$Fe_2(L\text{-}L) + H_2EDTA^{2-} + H^+ \rightleftharpoons Fe(EDTA)^- + Fe(L\text{-}H_3L) \quad (12b)$$

Equilibrium quotients (K_{eq}) of eqs 12a and 12b are expressed by eqs 13a and 13b and determined from the stoichiometry of the reactions performed.

$$K_{eq1} = [Fe(EDTA)^-][H_3L\text{-}H_3L]/[Fe(L\text{-}H_3L)][H_2EDTA^{2-}][H^+] \quad (13a)$$

$$K_{eq2} = [Fe(EDTA)^-][Fe(L\text{-}H_3L)]/[Fe_2(L\text{-}L)][H_2EDTA^{2-}][H^+] \quad (13b)$$

Equations 14a and 14b may be derived from eq 11, that for $Fe(EDTA)^-$, and eq 13.

$$K_{Fe(L-H_3L)} = (K_{Fe(EDTA)}/K_{eq1})(K_{av}^3/K_1^{edta}K_2^{edta}) \quad (14a)$$

$$K_{Fe_2(L-L)} = (K_{Fe(EDTA)}/K_{eq2})(K_{av}^3/K_1^{edta}K_2^{edta}) \quad (14b)$$

We used the following relations for derivation: $[H_3L\text{-}L^{3-}] = K_1K_2K_3[L\text{-}L^{6-}][H^+]^3$; $[H_3L\text{-}H_3L] = K_4K_5K_6[H_3L\text{-}L^{3-}][H^+]^3$; and $[H_2EDTA^{2-}] = K_1^{edta}K_2^{edta}[EDTA^{4-}] \times [H^+]^2$. However, the use of these relations means that we presume the following: protonation of the six hydroxamates takes place in the order of the upper site and then the lower site, and proton dissociation of $Fe(L\text{-}H_3L)$ occurs as expressed by $[Fe(L\text{-}H_3L)] = K_1K_2K_3[Fe(L\text{-}L)^{3-}][H^+]^3$. In practice, $Fe(L\text{-}H_3L)$ in eqs 11a, 12a, and 13 needs to be replaced by Fe_1-**2**, in which iron may reside at either site. Errors due to such ambiguous residency are less than 10%, since a probability of 93% at the lower and 7% at the upper site was determined using eq 8 above. Accordingly, we used the average K_{av} value for each K_n in our calculations, neglecting small differences between the presumed and the real protonation situations. The results are summarized in Table 4.

Discussion

Ligands and Complexes. The ditopic ligands (represented by **5** in Chart 1) and their Fe(III) complexes were previously reported to have intramolecularly hydrogen-bonded networks in chloroform.[19,21] However, their lipophilic nature and deoxygenated hydroxamate portions and the different ϵ values at the two binding sites rendered it inconvenient to make detailed kinetic and thermodynamic analyses of iron complexation in aqueous solution. Besides, their moderate CD intensity suggests that their iron complexes either have a lower helix content or contain a minor component of the optical antipode, owing to the less demanding regulatory effect of the backbone.

The present ligands (**1** and **2**) and their complexes (Ga-**1** and Ga_1-**2**) do not assume any particular, intramolecularly hydrogen-bonded structures in a polar solvent like DMSO, despite their peptide nature. This is indicated by large negative values of the temperature dependence of amide-proton chemical shifts. Consequently, in much more polar solvent, water, **1** and **2** are also not preorganized for complexation,[48] and their Fe(III) complexes are not stabilized by intramolecular hydrogen bonding. It is important, however, to use aqueous systems in determining the properties of iron complexes because of their relevance to biological systems as well as aqueous chemistry.

Ligand **2** has two discrete binding sites, and each binding site contributes to an equal ϵ value/Fe(III) at λ_{max}. The observed isosbestic behavior and related Schwarzenbach plots indicate that iron is accommodated at individual binding sites, ruling out the possibility of forming complicated polymeric complexes. The CD intensity observed for Fe_1-**2** and Fe_2-**2** suggests a high local symmetry of the chiral binding site. The 2-fold intensity of Fe_2-**2** to Fe_1-**2** is consistent with two similar, separate binding sites. Steric interaction between the CH_3 group of the L-Ala-$N(O^-)$ moiety and the β-CH_2 group of the NCH_2CH_2CO residue at the binding site forces iron(III) to coordinate in the Δ-*cis* configuration. Repetitive extension of the Ala-Ala-β-(HO)Ala unit appears to result in high CD intensity/Fe(III) of Fe_1-**2** and Fe_2-**2** relative to that of Fe-**1**, as in that of Fe-**3** and Fe-**4** (Table 1). The three supporting strands are forced locally to assume a triple-helical orientation in Fe_2-**2**, and the intervening peptide backbone links the two binding sites in a helical manner, resulting in a well-defined ditopic chiral complex. A proposed structure for the overall geometry of Fe_2-**2** is depicted, aided by a molecular model examination (Figure 6); similar structures are also possible for FeM-**2**, in which M replaces Fe. The tren moiety has an extended conformation with the nitrogen electron pair having an inward direction, unlike that shown for Fe_2-**5**.[19]

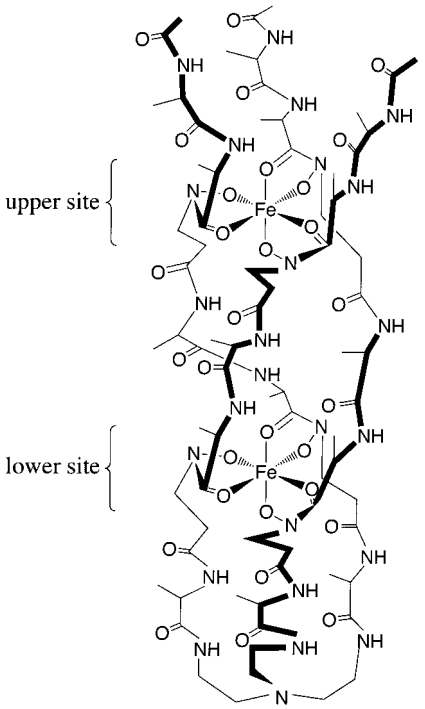

Figure 6. Proposed structure of Fe_2-**2** shown in the Δ-*cis* configuration. Similar structures for FeM-**2** are possible by replacing Fe with M.

Iron Loading. The sequence of eq 4 consists of several elementary steps, as shown by representative species, and appears to be complex; eq 4a involves dissociation of Fe(III)−oxalate and association of Fe(III)−hydroxamate together with their stepwise intermediary transformation, and eq 4b includes additional dissociation of M(III)−hydroxamate and association of M(III)−oxalate. The fact that exact 1- or 2-equiv amounts of the ferric oxalate virtually transformed M(L) to Fe(L) is ascribable to the outstanding stability of Fe(L) among M(III)−hydroxamate and M(III)−oxalate complexes.[49−51] A primary purpose for the experiments is to detect any difference in iron-loading rates for the different M(III)-preloaded ligands. The rate constants obtained by applying the second-order reaction models, therefore, are useful for discussing the formation process of Fe(L), even though they are apparent constants, and it is not known which step is rate-determining among those processes.

(48) Cram, D. J. *Science* **1988**, *240*, 760−767.

(49) The logarithmic stability constants of tris(hydroxamato)metal(III) complexes, to cite one example, for deferriferrioxamine B (= L), are as follows:[34] Al^{3+}(L), 24.14; Ga^{3+}(L), 28.17; In^{3+}(L), 20.60; Fe^{3+}(L),[32] 30.60.

(50) For L = oxalato:[45] (a) $Fe^{3+}(L)_3$, 18.49: (b) $Al^{3+}(L)_3$, 15.21; $Ga^{3+}(L)_3$, 17.86; $In^{3+}(L)_3$, 14.53: (c) For example, L^1 = acetato:[45] $In^{3+}(L^1)_3$, 7.9; $Fe^{3+}(L^1)_3$, 8.3.

(51) Martell, A. E.; Smith, R. M. *Critical Stability Constants*; Plenum Press: New York, 1974−1989; Vol. 1−6.

Scheme 3

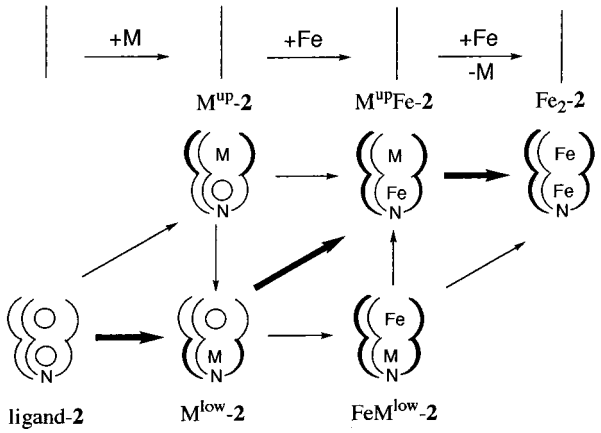

The absorbance change versus time curves clearly show different rates for the different M(L) complexes under similar reaction conditions (Figure 3, A and B). The different rates strongly suggest that dissociation of M(III)−hydroxamate plays a crucial role. The iron distributions in the 1-equiv loading on M_1-**2** (Table 3) indicate that the residing metal ion scrambles with the incoming iron for a formally vacant site (vide infra). A single rate constant for 2-equiv loading on **2** or In_1-**2** suggests that Fe(III) competes for the two binding sites with Fe(III) or In(III) throughout the reaction. Worthy of note is that the loading rate on In_1-**2** was faster (ca. 3 times) than the loading rate on the free ligand **2**.[52] An apparent rate constant is larger for 1-equiv loading than 2-equiv loading on In_1-**2** (entry 3c, Table 2). This is largely due to a different iron concentration, and, in fact, it is seen that 2-equiv loading was complete faster at 1-equiv iron stage (at absorbance 0.14 in Figure 3B).

In the loading on **2** (Scheme 3), there are two main pathways which are considered to be major and minor. A major pathway (shown by bold-face lines) leading to the product starts with M^{low}-**2**, as Ga(III) resides at the lower site. One-equivalent loading on this produces FeM-**2**, in which Fe(III) enters rather the lower site (Table 3, 75−79%) and the next 1-equiv loading affords Fe_2-**2**, expelling M(III) at the same time. A minor pathway, which is the rest of the pathway, is also open for Al_1-**2** and Ga_1-**2**, in which Fe(III) first enters the upper site (21−25%), as also suggested by similar rates for the two, and then exchanges with M(III) in the ligand. Upon the second iron coming in, M(III) dissociates as a key step, and Fe_2-**2** is produced.

Iron Removal. The hyperbolic dependence of both constants k_1^{up} and k_1^{low} on the EDTA concentration is consistent with the reaction sequence of eq 6,[16] where an intermediate ternary complex is formed, as previously discussed by Albrecht-Gary et al.[46] and recently by us.[47] With Fe_2-**2**, for example, a value of k_1^{up} is faster than that of k_1^{low} (a factor of 5 in entry 4a in Table 3, and also compare two k_{max} values).

Rate constants k_1^{low} obtained for Fe_1-**2** through the parallel first-order kinetics and for FeM-**2** through the consecutive first-order kinetics converge at a value of 4.0×10^{-3} s^{-1} determined for the rate constant k_1^{low} of Fe_2-**2** (entries 4b and 5a∼5c in Table 3). This coincidence is reasonable, since the same situation common to all of the complexes is left after removal of the upper metal ion.

A preference for iron residence at the lower site is exhibited by a distribution of Fe_1-**2** (lower/upper; 93/7), which is in line with the NMR data of Ga_1-**2**. Similar preference for the lower site is also shown in the distributions of FeM-**2** in which a large portion of iron (75∼79%) resides at the lower site.

The observed iron-removal rates are much faster than that for ferrichrome (6.1×10^{-4} s^{-1}) under comparable conditions.[17c] This trend is similar to that observed for previous peptide hydroxamate ligands.[47]

Although iron prefers to reside at the lower site, iron may migrate from the lower to the upper site. Even when this migration occurs during an iron-removal reaction, the migration rate is included in the constant k_1^{low}.

When we consider a global iron mobilization sequence, the above-described behavior illustrates that iron is captured by the ligand, stored mostly at the lower site, and then released from the storage site by a scavenger, EDTA, only after the upper M(III) release.

Stability Constants. The values of the constant $K_{Fe(HL)}$, which represents the monoprotonation stability, increase in the order, ferrichrome < Fe-**1** < Fe_1-**2** < Fe-**3** < Fe_2-**2** < Fe-**4** with the decreasing stability of Fe(L). We interpret this order as reflecting the increasing strain present in these complexes. When we compare them on a monoiron basis, the tren-based tripodal structure appears to produce flexible complexes relative to those of **3** and **4**.

For the first time, the proton-independent stability constants for Fe_2-**2** were obtained via the determination of iron residence probability in Fe_1-**2**. The stability constants at the lower site of Fe_1-**2** and the upper site of Fe_2-**2** are almost the same order as that of Fe-**1** and also the same as those of Fe-**3** and Fe-**4**. All of these stability constants are close to that of ferrichrome (Table 4). However, iron preference for the lower site is not apparent in these values; the constant for the upper site of Fe_2-**2** is only determinable in the presence of iron at the lower site.

Conclusions

The monotopic and ditopic ligands **1** and **2** prepared were not preorganized for complexation, and the formed iron(III) complexes were not stabilized by intramolecular hydrogen bonding in a solvent like DMSO and, of course, not in much more polar solvent water. Nevertheless, ligands **1** and **2** afforded well-defined, chiral iron(III) complexes in water, as shown by CD spectroscopy, ESIMS, and isosbestic behavior on UV−vis spectra. Iron loading on ligand **2** or on the M(III)-preloaded ligands with ammonium ferric oxalate was found to proceed through Fe(III) and M(III) competition, suggesting that dissociation of the M(III)−hydroxamate bond is a crucial factor for the rate. In general, the rate of iron loading on M(III)-preloaded ligands increased in the order Al < Ga < Fe < In. Iron-removal reactions of the formed complexes under the pseudo-first-order kinetic conditions with EDTA reflect the states of iron residence in **2**. The two rate constants for iron removal from Fe_2-**2**, k_1^{up} and k_1^{low}, were determined, and the iron residence preference for the lower site in Fe_1-**2** and in FeM-**2** was noted. The processes of iron loading and its subsequent removal, when viewed as an iron-holding host ditopic ligand coupled with a competing guest molecule, represent a complex iron-mobilization system. We envisage iron mobilization such as this, although ligating functional groups are different, in intracellular intricate processes which are not yet well-characterized.[1] The present ditopic ligand serves as an abiotic iron-storing vehicle and provides a means for studying iron mobilization in aqueous systems.

Experimental Section

General Procedures. IR spectra were obtained on a JASCO model A-302 spectrophotometer, and UV−vis spectra were recorded on a

(52) We thought this was due to a preorganization effect of the ligand for Fe(III) loading with In(III), although a reviewer disagreed with our view.

Hitachi 320A spectrophotometer. CD spectra were taken with a JASCO J-720 spectrophotometer. HPLC was carried out on a JASCO 880-PU apparatus combined with 875-UV and 100-III attachments, using a column (4.6 mm × 250 mm) of CrestPak C18 T-5. A solvent system of CH_3CN-H_2O (3:1 v/v) containing 0.1% phosphoric acid and 5 mM sodium 1-octanesulfonate was applied at a flow rate of 1 mL/min, and the retention time (R_t) was determined. Mass spectra were determined on Micromass QUATTRO II equipment. Optical rotations were measured with a Horiba SWPA-2000 polarimeter at 25 ± 0.1 °C. ^{1}H NMR spectroscopy was performed in $CDCl_3$ at an ambient temperature or in DMSO-d_6 with a JEOL GX-400 or an A-500 spectrometer using Me_4Si as the standard. The melting points are uncorrected. Double-distilled water was deionized by passing through an ion-exchange resin (Dowex 50W-X8).

Synthesis. Boc-Ala-Ala-β-(BnO)Ala-OH (**6a**) was obtained as previously reported.[28]

(Boc-Ala-NHCH$_2$CH$_2$)$_3$N (7a). To a mixture of Boc-Ala-OH (6.81 g, 36 mmol), HOBt (6.12 g, 40 mmol) and EDC·HCl (9.59 g, 50 mmol) in CH_2Cl_2 (100 mL) was added tris(2-aminoethyl)amine (1.46 g, 10 mmol) in DMSO (10 mL). The mixture was stirred for 3 h at −10 °C and for 50 h at room temperature, and the solvent was evaporated, followed by addition of $CHCl_3$ (100 mL). The resulting mixture was washed with water (2 × 50 mL) and 5% aqueous $NaHCO_3$ (3 × 100 mL) and dried ($MgSO_4$). Evaporation of the solvent and tritiation of the residue with $CHCl_3-$EtOAc gave crystals of **7a** (3.78 g, 57%): mp 162−163 °C; IR (KBr, cm^{-1}) 3300, 2900, 1700 (C═O Boc), 1670 (C═O amide), 1535 (NH amide), 1370, 1250, 1175; ^{1}H NMR ($CDCl_3$) δ 1.36 (d, J = 7.1, 9H), 1.42 (s, 27H), 2.56 (t, 6H), 3.00−3.50 (m, 6H), 4.40 (m, 3H), 5.60 (br d, 3H), 8.78 (br s, 3H).

[Boc-Ala-Ala-β-(BnO)Ala-Ala-NHCH$_2$CH$_2$]$_3$N (8a). Compound **7a** (4.67 g, 7.09 mmol) was treated in TFA (130 mL, 1.7 mol) for 3.5 h at 0 °C to give tris(CF_3CO_2H·H−Ala-$NHCH_2CH_2$)N (**7b**) as an oil with inclusion of TFA (9.95 g, 7.09 mmol). To a mixture of **6a** (11.7 g, 24.8 mmol), HOBt (6.13 g, 40 mmol), and EDC·HCl (7.67 g, 40 mmol) in $CHCl_3$ (100 mL) was added dropwise **7b** and NMM (7.14 mL) in DMSO (30 mL) at −10 °C. The mixture was stirred for 3 h at −10 °C and for 24 h at room temperature, followed by addition of $CHCl_3$ (100 mL). The resulting mixture was washed with water (2 × 200 mL) and aqueous 5% $NaHCO_3$ (3 × 200 mL) and dried ($MgSO_4$). After evaporation of the solvent, the residue was purified by silica gel chromatography with $CHCl_3-$MeOH (5:1 v/v), yielding a product (**8a**) (10,4 g, 91%): HPLC R_t 3.0 min; IR (KBr, cm^{-1}) 3300, 2970, 1650, 1530, 750, 700; ^{1}H NMR (DMSO-d_6 at 40 °C) δ 1.15 (m, 27H), 1.38 (s, 27H), 2.45 (m, 12H), 3.08 (m, 6H), 3.72−4.04 (m, 6H), 4.05 (m, 3H), 4.28 (m, 3H), 4.85 (m, 3H), 4.95 (ABq, J = 9.2, 6H), 6.80 (br s, 3H), 7.41 (m, 15H), 7.70 (t, J = 6.4, 3H), 7.93 (d, J = 7.3, 3H), 8.05 (d, J = 7.1, 3H).

[Ac-Ala-Ala-β-(BnO)Ala-Ala-NHCH$_2$CH$_2$]$_3$N (8c). Compound **8a** (1.62 g, 1.00 mmol) and TFA (20 mL, 240 mmol) in CH_2Cl_2 (20 mL) were treated for 3 h at 0 °C, and evaporated. A residue (**8b**) was treated with Et_3N (4.0 mL) in DMSO (5.0 mL) and *N*-acetoxysuccinimide[53] (0.94 g, 6.0 mmol) in $CHCl_3$ (20 mL) for 3 h at −10 °C and for 50 h at room temperature and purified by silica gel chromatography with $CHCl_3-$MeOH (5:1 v/v) to give a compound **(8c)** in 84% (1.21 g): HPLC R_t 7.7 min; IR (KBr, cm^{-1}) 1650, 1540, 750, 700; ^{1}H NMR (DMSO-d_6 at 40 °C) δ 1.15 (m, 27H), 1.83 (s, 9H), 2.45 (m, 12H), 3.08 (m, 6H), 3.70−4.00 (m, 6H), 4.32 (m, 6H), 4.85 (s, 3H), 4.95 (m, 6H), 7.40 (m, 15H), 7.71 (t, J = 6.5, 3H), 7.93 (d, J = 7.8, 3H), 8.04 (d, J = 7.8, 3H), 8.08 (d, J = 7.8, 3H).

[Ac-Ala-Ala-β-(HO)Ala-Ala-NHCH$_2$CH$_2$]$_3$N (1). Compound **8c** (0.40 g, 0.28 mmol) in MeOH (50 mL) was hydrogenated with H_2 in the presence of Pd on carbon (100 mg; 10%) for 24 h and filtered, and the solvent was evaporated. The product was purified with a Sephadex LH-20 column to give a white solid (0.20 g, 61%): HPLC R_t 3.8 min; Optical rotation $[\alpha]^{25}_D$ − 83 (*c* 0.3, H_2O); IR (KBr, cm^{-1}) 3300 (*N*−OH), 1650 (CO amide) 1540, 1380, 1120; ^{1}H NMR (DMSO-d_6 at 30 °C) δ 1.17 (d, J = 7.3, 9H), 1.20 (d, J = 7.3, 18H), 1.83 (s, 9H), 2.41 (t, J = 7.0, 6H), 2.50 (br d, J = 6.5, 6H), 3.10 (m, 6H), 3.71 (m, 6H), 4.23 (qn, J = 7.3, 3H), 4.30 (qn, J = 7.3, 3H), 4.79 (qn, J = 7.3, 3H), 7.79 (t, J = 5.1, 3H), 7.80 (d, J = 7.2,3H), 7.99 (d, J = 7.8, 3H), 8.09 (d, J = 7.0, 3H), 9.95 (s, 3H). Anal. Calcd for $C_{48}H_{84}N_{16}O_{18}$·4H_2O: C, 46.29; H, 7.45; N, 18.00. Found: C, 46.49; H, 7.26; N, 18.33.

[Ac-Ala-{Ala-β-(HO)Ala-Ala}$_2$-NHCH$_2$CH$_2$]$_3$N (2). Compound **8a** (0.51 g, 0.31 mmol) in CH_2Cl_2 (1.0 mL) was treated with TFA (14.3 mL, 187 mmol) at 0 °C for 3.5 h, and the solvent was evaporated. A residue (**8b**) in DMSO (10 mL) was condensed with **6a** (0.57 g, 1.3 mmol) in DMF (13 mL) in the presence of NMM (0.39 mL, 3.5 mmol) for 3 h at 0 °C and for 24 h at room temperature by a BOP reagent[54] (0.88 g, 2.0 mmol) accompanied with NMM (0.33 mL, 3.0 mmol). DMF was evaporated, and $CHCl_3$ (100 mL) was added. The mixture was washed with water (2 × 50 mL), 5% aqueous $NaHCO_3$ (3 × 100 mL), dried ($MgSO_4$), and purified by a Sephadex LH-20 column (with MeOH) to give a product: {**Boc-Ala-[Ala-β-(BnO)Ala-Ala]$_2$-NHCH$_2$CH$_2$**}$_3$**N (9a)** in 80% (0.64 g): HPLC R_t 8.0 min; IR (KBr, cm^{-1}) 1680, 1640, 1540, 1450, 1370, 750, 700; ^{1}H NMR ($CDCl_3$) δ 1.25 (m, 45H), 1.43 (s, 27H), 2.47 (m, 18H), 2.9−3.3 (m, 6H), 3.8−4.1 (m, 12H), 4.25 (m, 3H), 4.58 (m, 6H), 4.93 (d, J = 7.1, 12H), 4.95 (m, 6H), 5.38 (br s, 3H), 7.00 (br s, 3H), 7.37 (m, 30H), 7.41 (br s, 6H), 7.60 (d, J = 6.6, 3H). Compound **9a** (0.597 g, 0.232 mmol) in CH_2Cl_2 (2.3 mL) and TFA (10.6 mL, 139 mmol) gave **9b**, which was acetylated in DMSO (1.0 mL)−$CHCl_3$ (15 mL) with *N*-acetoxysuccinimide (0.182 g, 1.16 mmol) and Et_3N (0.54 mL) at −10 °C for 3 h and for 24 h at room temperature. The residue obtained was purified by a Sephadex LH-20 column (with MeOH) to give a product (0.35 g, 63%): {**Ac-Ala-[Ala-β-(BnO)Ala-Ala]$_2$-NHCH$_2$CH$_2$**}$_3$**N (9c)**: HPLC R_t 7.2 min; IR (KBr, cm^{-1}) 1660, 1640, 1540, 1450, 1370, 750, 700; ^{1}H NMR (400 MHz, $CDCl_3$) δ 1.24 (m, 45H), 1.96 (s, 9H), 2.46 (m, 12H), 2.53 (m, 6H, s), 2.9−3.3 (m, 6H), 3.7−4.2 (m, 12H), 4.57 (m, 9H), 4.88 (s, 12H), 4.93 (m, 6H), 6.80 (br s, 3H), 7.28 (br s, 3H), 7.36 (m, 30H), 7.64 (br s, 12H). Compound **9c** (0.15 g, 0.063 mmol) in MeOH (100 mL) was hydrogenated with H_2 in the presence of Pd on carbon (15 mg, 10%) for 20 h at room temperature. The product (**2**) was purified with a Sephadex G-15 column to afford a white solid (60 mg, 52%): HPLC R_t 2.1 min; Optical rotation $[\alpha]^{25}_D$ −60 (*c* 0.3, H_2O); IR (KBr, cm^{-1}) 3260 (*N*−OH), 1640, 1540, 1450 (CONOH); ^{1}H NMR (DMSO-d_6 at 30 °C) δ 1.17 (d, J = 6.8, 27H), 1.19 (d, J = 5.4, 18H), 1.83 (s, 9H), 2.40 (t, J = 6.5, 18H), 3.10 (m, 6H), 3.69 (m, 12H), 4.27 (qn, J = 7.0, 3H), 4.29 (qn, J = 7.3, 6H), 4.78 (qn, J = 6.6, 6H), 7.79 (t, J = 6.5, 3H), 7.84 (d, J = 7.3, 6H), 7.98 (d, J = 7.3, 3H), 8.09 (d, J = 7.3, 6H), 9.91 (s, 6H). Anal. Calcd for $C_{75}H_{129}N_{25}O_{30}$·6.5$H_2O$: C, 45.54; H, 7.24; N, 17.70. Found: C, 45.68; H, 6.93; N, 17.38.

Iron(III) Complex Formation. Stock solutions of 3.05 × 10^{-3} M and 1.47 × 10^{-3} M for ligands **1** and **2** in water were prepared. A stock solution of ferric nitrate (2.93 × 10^{-3} M) was prepared by dissolving $Fe(NO_3)_3$·9H_2O in 0.1 M nitric acid solution.

(a) In a 10-mm cell held at a constant temperature of 25.0 ± 0.1 °C in the cell compartment of the spectrophotometer, a solution of **1** (7.84 × 10^{-7} mol) and a KCl solution were placed and diluted with water. The total volume was 3.00 mL with 0.10 M KCl. In the case of **2**, a ligand solution (3.9 × 10^{-7} mol) was used to make a 3.00 mL solution with 0.10 M KCl. To these was added an iron(III) solution (7.82 × 10^{-7} mol). The pH of the solution was determined (pH 2.1 ± 0.1).

For studies at pH 7.0, the pH of the solutions was adjusted with 0.1 M KOH (ca. 0.3 mL). The CD spectrum was determined for this solution, and the concentration was corrected for added volume.

(b) For pH titration studies, the pH of the above neutral solutions was adjusted with small quantities of either 0.1 M HNO_3 or 0.1 M KOH. The UV−vis spectra were recorded, and the concentrations of the resulted solutions were corrected for added volume.

(c) Schwarzenbach plots were generated from these solutions that exhibited isosbestic behavior in the UV−vis spectra during the pH titration studies.

NMR Determinations of Gallium(III) Complexes. A 1.5-equiv or a 1.0-equiv amount of $Ga(OH)_3$, prepared in situ from $Ga(NO_3)_3$ and aqueous alkali, was combined with **1** or **2** in H_2O, respectively, stirred for 24 h, and filtered, and the solution was evaporated. The solid was dissolved in DMSO-d_6.[15] Alternatively, Ga_1-**2** was prepared in situ by

(53) Castro, B.; Dormoy, J. R.; Evin, G.; Selve, C. *Tetrahedron Lett.* **1975**, 1222−1225.

(54) Lindsay, D. G.; Shall, S. *Biochem. J.* **1971**, *121*, 737−745.

combining equimolar amounts of **2** and tris(acetylacetonato)Ga(III) in DMSO-d_6 and allowing the solution to equilibrate for 2 days. The degree of Ga loading was estimated to be 90% in the latter case. Complex Ga_1-**2** was soluble in water and DMSO, and separable from insoluble complex Ga_2-**2**.

Al(III), Ga(III), and In(III) Complexes. In a 10-mm UV−vis cell, a ligand solution (both 3.9×10^{-7} mol) was mixed with an aqueous metal(III) ion solution (3.9×10^{-7} mol) prepared from $AlCl_3$ (3.71×10^{-2} M), $Ga(NO_3)_3$ (1.44×10^{-2} M), or $In(NO_3)_3$ (8.71×10^{-3} M), respectively. Each acidic mixture (ca. pH 2) was neutralized to pH 7.0 with KOH (0.1 M) solution and diluted with water to make a solution of 2.86 mL, half (1.43 mL, 1.95×10^{-7} mol) of which was used each time. Metal(III) ion complex formation was confirmed by the absence of insoluble metal hydroxides at pH 7.

For an iron-removal run, the above acidic mixture (pH 2) was diluted with water to 2.56 mL, half (1.28 mL) of which was used each time.

Kinetics for Iron(III) Loading. In a 10-mm cell were mixed a buffer solution (1.50 mL) of pH 5.4 (AcOH−AcONa, 0.20 M, maintained at $I = 0.20$ with KCl), and the above aqueous solution (1.43 mL, 1.95×10^{-7} mol) containing **1** or **2**. In the case of a metal(III)-preloaded solution, each of the above prepared solutions of M-**1** or M_1-**2** (1.43 mL) in a cell was mixed with this buffer solution. To each of these combined solutions (2.93 mL) was added a solution (0.064 mL, 1.95×10^{-7} mol) of $Fe(C_2O_4)_3 \cdot (NH_4)_3 \cdot 3H_2O$ to initiate a 1-equiv iron-loading reaction. For 2-equiv loading, a solution of 3.90×10^{-7} mol was added.

Ammonium ferric oxalate remained intact at least hours under the experimental conditions, although much less stable than ferric hydroxamates. Formation of iron(III) complexes with respect to iron(III) and ligand (or metal-loaded ligand) was followed by monitoring an increase in absorbance at 425 nm with time (over 60 s), and the rate was determined by plotting the data according to the second-order kinetic equation, $[A_t\epsilon / A_\infty(A_\infty - A_t)] = k_{2_{app}}t$. An excellent linear plot was obtained for more than three half-lives. The rate constant was an average of at least two determinations and contains errors of ±10%.

As a sample of an iron-removal run, a buffered FeM-**2** solution (2.844 mL) in a cell was obtained, by mixing the above M_1-**2** solution (1.28 mL), the buffer solution (1.50 mL), and the iron solution (0.064 mL). These solutions were used in 1 and 24 h after mixing, respectively. A solution (2.844 mL) of Fe-**1**, Fe_2-**2**, or Fe_1-**2** was similarly obtained.

Electrospray Ionization Mass Spectrometry. Ferric hydroxide was obtained by neutralizing an aqueous ferric chloride solution with NaOH to pH 7.0. The precipitates were separated and washed with water. Ligand **2** and excess $Fe(OH)_3$ (precipitates) were stirred together in water for 50 h and filtered. A sample was obtained by evaporation of the filtrate.

For an FeM-**2** sample, 1 equiv of M(III) hydroxide (M = Al, Ga, and In) was similarly prepared as precipitates, and a mixture of **2** and the precipitate was stirred in water to give an M_1-**2** solution, and then 1 equiv of ferric ammonium oxalate was added to this solution. These FeM-**2** solutions were used directly for ES-MS determinations. Samples of FeIn-**2** were measured within a few hours after preparation.

ESI cone voltage, + 30 V. Fe_2-**2** *m/z*: $[Fe_2\text{-}\mathbf{2} + H_2O + 3H]^{3+}$, 661.6; $[Fe_2\text{-}\mathbf{2} + Na + H]^{2+}$, 995.1; $[Fe_2\text{-}\mathbf{2} + 2Na]^{2+}$, 1006.1; $[Fe_2\text{-}\mathbf{2} + Na]^{+}$, 1989.9. FeAl-**2** *m/z*: $[FeAl\text{-}\mathbf{2} + Na + H]^{2+}$, 980.7; $[FeAl\text{-}\mathbf{2} + 2Na]^{2+}$, 992.3; $[FeAl\text{-}\mathbf{2} + Na]^{+}$, 1960.0. FeGa-**2** *m/z*: $[FeGa\text{-}\mathbf{2} + Na + H]^{2+}$,-1001.8; $[FeGa\text{-}\mathbf{2} + 2Na]^{2+}$, 1021.3; $[FeGa\text{-}\mathbf{2} + 2H_2O + Na + H]^{2+}$, 1019.7. FeIn-**2** *m/z*: $[FeIn\text{-}\mathbf{2} + H_2O + Na]^{+}$, 2065.9: ESI cone voltage, − 15 V. FeIn-**2** *m/z*: $[FeIn\text{-}\mathbf{2} + 2OH]^{2-}$, 1028.9; $[FeIn\text{-}\mathbf{2} + 2H_2O + 2OH]^{2-}$, 1046.5.

Rates of Iron(III) Removal by EDTA. To initiate a reaction, EDTA (0.156 mL, 3.9×10^{-3} mol to become 1.3×10^{-3} M) was added to each of the buffered FeM-**2**, Fe_1-**2**, and Fe_2-**2** solutions (2.844 mL, 1.95×10^{-7} mol) in a cell at 25.0 °C. The reaction was monitored at 425 nm to give absorbance changes versus time curves. The collected data were analyzed by the curve-fitting procedure using eqs 7, 8, or 9, respectively (see text), to generate first-order rate constants, k_1^{up} and k_1^{low}. The reaction was duplicated for reproducibility. The limits of estimated deviations were determined through the same curve fits (±20% for k_1^{up} and ±5% for k_1^{low}).

For the case of Fe-**1** (1.3×10^{-4} M), a solution of EDTA (2.6×10^{-3} M) was used. A pseudo-first-order rate constant for Fe-**1** was obtained from a semilogarithmic plot of absorbance versus time, the reaction being followed more than three half-lives. The observed rate (k_{obs}) was obtained as an average value with error limits of ±5%.

Determination of p*K*'s. Potentiometric titration was performed by a previously described procedure.[28] The p*K*'s of **1** and **2** were calculated using programs PKAS and HYPERQUAD,[55,56] with $\sigma < 0.01$ for **1** and $\sigma < 0.05$ for **2**. The p*K* value was an average of two determinations with error limits of ±0.05 p*K* unit.

Equilibrium Competition Reactions With EDTA. The reactions were carried out essentially by the same procedure previously reported.[28]

Acknowledgment. We thank Dr. Kazuhisa Hiratani of the National Institute for Advanced Interdiciprinary Research for his courtesy in taking measurements of mass spectrometry.

Supporting Information Available: Table S1: ^{1}H NMR data of ligands **1** and **2** (PDF). This material is available free of charge via the Internet at http://pubs.acs.org.

JA003251G

(55) Martell, A. E.; Motekaitis, R. J. *Determination and Use of Stability Constants*, 2nd ed.; VCH Publishers: New York, 1992.

(56) Gans, P.; Sabatini, A.; Vacca, A. *Talanta* **1996**. *43*, 1739−1753.